conventional therapies and were not optimal candidates for surgical or catheter revascularization. Buerger's disease was diagnosed by segmental occlusion of small- and medium-sized arteries, absence of atherosclerosis, and corkscrew collaterals circumventing the occlusion in angiogram and the exclusion of autoimmune diseases such as scleroderma or systemic lupus erythematosus, hypercoagulable states, diabetes, or acute arterial occlusion secondary to embolism. Patients with retinopathy and/or malignancy were excluded. Although 30 patients with atherosclerotic peripheral artery disease were candidates for BMT, they were excluded from the present study due to their systemic atherosclerotic complications. Six patients with Buerger's disease were recruited for the present study. All patients had legs pain at rest and five patients had foot ulcers. Written consent was obtained from all participants of this study. This clinical trial of autologous BMT for the treatment of patients with critical ischemia was approved by the Medical Ethics Committee of the National Cardiovascular Center.

Autologous BMT

Bone marrow fluid (700-800ml) was collected from the iliac bone under general anesthesia. The harvested bone marrow fluid was diluted with RPMI 1640 (Nikken Bio Medical Laboratory, Kyoto, Japan) containing heparin, then stored in a sterile pack from the Bone Marrow Collection Kit (Baxter, IL, USA). The mononuclear cell fraction was prepared with a Fresenius AS104 (AMCO, USA). The injection volume was 0.5ml and injections were spaced 2-3cm apart, using a 1ml syringe and a 27-gauge needle. Leg pains were measured by a visual analog pain scale and foot ulcers were evaluated by area and appearance.

Novel micro-angiography

The in-hospital micro-angiographic equipment consisted of a high power X-ray source for computed tomography and an avalanche type detector characterized by a high spatial resolution (20μm) and high sensitivity (100 times of CCD camera) (Fig.1).

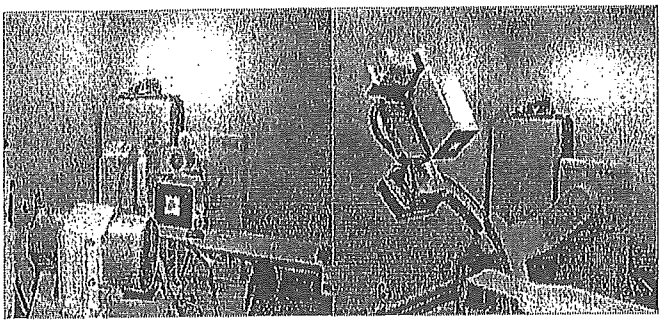

a b

Fig. 1a, b. The micro-angiographic equipment that we developed. High-voltage power X-ray source **a** and a detecting system with a high spatial resolution(25μm) and high sensitivity (100 times of CCD camera) **b.**

Limb ischemia models in rabbits were made by ligating the femoral artery and treated by fibroblast growth factor 4 (FGF-4) genes incorporated to gelatin hydro gel (GHG). One month after the treatment, we evaluated collateral micro-vessels by using conventional and micro-angiographic systems. The approach was via the left femoral artery so that the catheter was located in the abdominal aorta. A 5ml bolus of Iodine contrast medium (300mg/ml) was injected at 3ml/sec using an auto-injection system. Imaging was recorded using a digital source in 1000 x 1000 pixels. The sum of radio-absorptions for 10 seconds in clinical settings was studied.

Results

Autologous BMT for Critical Limb Ischemia

The number of transplanted bone marrow mononuclear cells were one to five multiplied 10^9. Rest pains decreased or disappeared in one month after BMT (Fig.2) and Skin ulcers improved in one to three months after BMT in all patients (Fig.3).

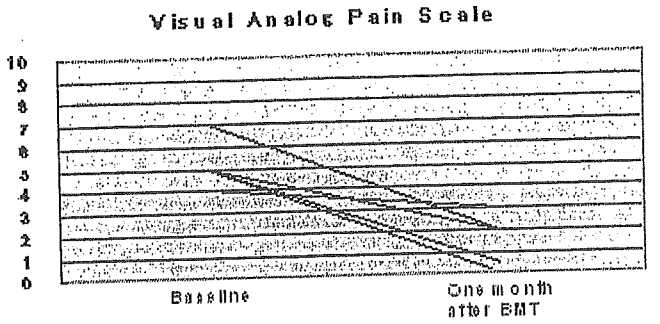

Fig. 2. The Visual analog pain scale in all patients.

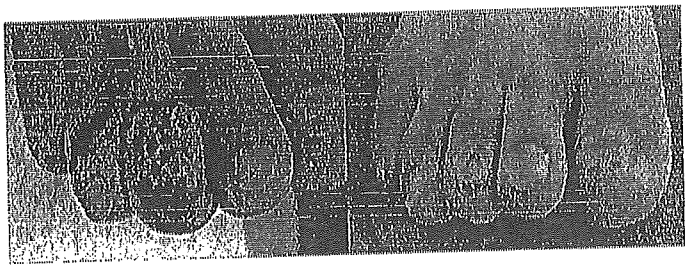

Fig. 3a, b. The skin ulcers in a patient before **a** and one month after autologous bone marrow transplantation **b**.

Conventional angiography was performed before and one month after BMT, but there was no significant changes in any of the patients (Fig.4).

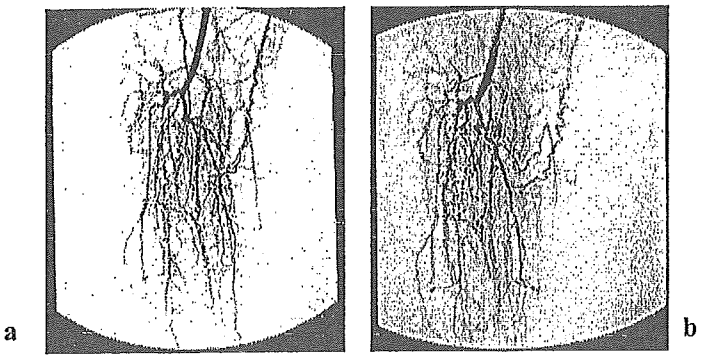

Fig. 4a, b. The conventional angiographic findings in the patient before **a** and one month after autologous bone marrow transplantation **b**.

Novel micro-angiography

The novel micro-angiography can detect to within a limit 50 of μm, although a detection limit of a conventional angiography is 250μm (Fig.5).

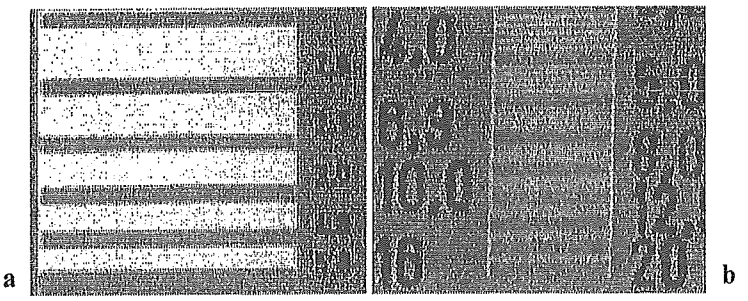

Fig. 5a, b. The detection limits on a conventional angiography **a** and the novel micro-angiography **b** using a line chart

Collateral micro-vessels, which were 100-500μm or less in diameter, were demonstrated more clearly in micro-angiography than conventional angiography (Fig.6).

The sum of radio-absorptions at the point of 1m distance from the X-ray source in clinical settings was 300 mSv. for 10 seconds.

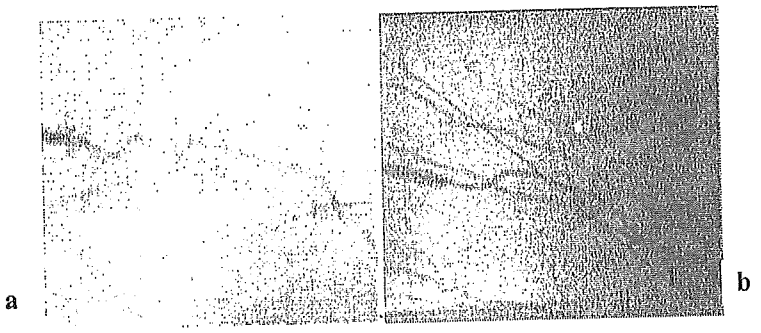

Fig. 6a, b. In 2.5x2.5cm view size, Collateral micro-vessels after therapeutic angiogenesis in the rabbit limb ischemia model. Vessel sizes in the range of 100-500μm or less, were demonstrated in the novel micro-angiography **b** more clearly than in a conventional angiography **a**. The diameter of the line in the micro-angiography is 130μm.

Discussion

Autologous BMT improved chronic severe limb ischemia due to Bue rger's disease. Conventional angiography could not disclose develope d collateral vessels after BMT. A novel micro-angiography technique could illuminate promoted collateral vessels after therapeutic angioge nesis in rabbit models although a conventional angiography did not. The sum of radio-absorptions in the novel angiography could be acc-epted in clinical settings.

Autologous BMT and Buerger's disease

Bone marrow harvests need an amount of more than 500ml bone marrow fluid and general anesthesia in therapeutic angiogenesis using BMT. Such factors have practical limitations to select candidates with peripheral artery disease complicated with systemic atherosclerosis and aging for BMT. Buerger's disease is a segmental vasculitis that affects the distal arteries of the upper and lower extremities. It typically occurs in young people. The majority of patients with Buerger's disease have pain at rest and digital

ulcerations and are hard to treat by revasculaizations, including catheter angioplasty and surgical bypass grafting, because of peripheral artery lesions. Patients with Buerger's disease, however, tend to have less systemic atherosclerotic lesions and normal cardiac function. These suggest that patients with Buerger's disease are the ideal candidates for therapeutic angiogenesis using autologous BMT.

Discrepancy between clinical improvements and conventional angiographic findings after BMT

BMT improved critical limb ischemia clinically. Promoted collateral vessels after the treatment were not, however, visualized well by conventional angiography. These vessels are quite small and the detection limit of small vessels by conventional angiography is about 200μm in diameter.

Novel micro-angiography

Recently, synchrotron radiation system characterized by high brightness, monochromatic and collimated nature bypass, revealed micro-vessels in situ. However the high cost of a synchrotron system strictly limits its clinical application (100 million dollars or more). We developed an in-house micro-angiographic system with a relatively low cost of approximately 1million dollars, which consisted of a high-voltage power X-ray source and a detecting system with a high spatial resolution (25μm) and high sensitivity (100 times of CCD camera). We evaluated collateral micro-vessels one month after therapeutic angiogenesis by using the conventional and micro-angiographic system. The in-house micro-vessel angiographic system could detect the micro-vessels more precisely than conventional angiographic system. We thought that the present micro-angiography should be useful for evaluating efficacy of therapeutic angiogenesis in clinical settings.

Conclusions

Conventional angiography failed to disclose the promoted collateral vessels after BMT although BMT improved the critical limb ischemia clini-

cally. The in-house micro-angiographic system could detect the micro-vessels more precisely than conventional angiographic system and the sum of the radio-absorption in the equipment could be acceptable in clinical settings. The novel in-house micro-angiographic system can be useful in the evaluation of therapeutic angiogenesis clinically.

References

Asahara T, Murohara T, Sullivan A, et al.(1997) Isolation of Putative Progenitor Endothelial Cells for Angiogenesis. Science 275:964-966

Iba O, Matsubara H, Nozawa Y, et al.(2002) Angiogenesis by Implantation of Peripheral Blood Mononuclear Cells and Platelets into Ischemic Limbs. Circulation 106:2019-2025

Inaba S, Egashira K, Komori K (2002) Peripheral-blood or bone-marrow mononuclear cells for therapeutic angiogenesis? Lancet 360:2083.

Shintani S, Murohara T, Ikeda H, et al.(2001) Augmentation of Postnatal Neovascularizaion with Autologous Bone Marrow Transplantation. Circulation 103: 897-903

Tateishi-Yuyama E, Matsubara H, Murohara T, et al.(2002) Therapeutic angiogenesis for patients with imb ischemia by autologous transplantation of bone-marrow cells:a pilot study and a randomised controlled trial. Lancet,360:427-35

4．画像解析-微小血管造影-

知久　正明・西上　和宏・内藤　博昭・盛　英三・佐藤　英一

狭心症や心筋梗塞などの虚血性心疾患や閉塞性動脈硬化症に対する新しい治療戦略として血管再生治療[用解1)]が期待されている。実際の臨床では，血管造影を含めた臨床検査で臨床症状の効果を十分には反映していない。これは，既存の血管造影装置の解像度は約200～300 μmであり，再生される新生血管は約100 μm以下の微小血管であるからである。微小血管造影の先駆けとなったシンクロトロンによる微小血管造影法[用解2)]は200～500 μm以下の微小血管の定量と50～200 μm以下の微小血管の可視化が可能である。さらに，臨床の場で簡便に使用できる微小血管造影装置も開発された。本稿では，再生治療後の微小血管の評価方法について概説する。

はじめに

血管再生には，一般に既存の血管から血管内皮細胞が増殖，リモデリングし，新しい血管枝が形成される狭義の血管新生（angiogenesis）と，血管内皮前駆細胞である血管芽細胞が集合・分化して血管が形成される血管発生（vasculogenesis）の2つが考えられている。血管発生は，主に胎生期に行われると考えられていたが，成人末梢血中のCD34陽性単核球の分画から血管内皮細胞へと分化しうる血管内皮前駆細胞（endothelial progenitor cell：EPC）があることが報告され，成人においても血管発生による血管再生が起こりうることが示された[1)2)]。特に単核球分画中で血管内皮細胞に分化しうる単核球は，主に骨髄に存在するため，動物実験の虚血モデルに骨髄単核球細胞移植をすることにより，血管新生や側副血行路が発達し，下肢血流量増加作用や心機能が改善することが確認された。これに基づき，重症下肢虚血患者に対し自己骨髄細胞移植や末梢血幹細胞移植が臨床導入され，良好な成績が報告されている[3)]。しかし，既存の血管造影装置では空間解像度が200 μm前後で，ミリメーターオーダーの血管を主たる観察対象としている。そのため，新生血管床の構築と機能の評価には極めて不十分といわざるを得ない。そこで，微小血管を観察できる微小血管造影法に期待がもたれている。

Ⅰ．微小血管造影法

1．放射光微小血管造影法

再生された微小血管を血管造影検査で評価するためには，微量の造影剤を検出できる装置が必要となる。その要素としてはX線の性質が高輝度で，平行性，単色性であり，なおかつ検出系が高感度，高解像度であることが重要である。これらの要素をすべて取り揃えているのが放射光施設内の微小血管造影装置である[4)]。放射光とは広域のスペクトルを持つ白色光であり，太陽光のように限りなく

Key words
微小血管造影，血管再生治療，新生血管，単色X線，放射光微小血管造影法，病院設置型微小血管造影法，プラズマX線微小血管造影法，angiogenesis，vasculogenesis，endothelial progenitor cell

図❶　X線エネルギーと質量吸収係数

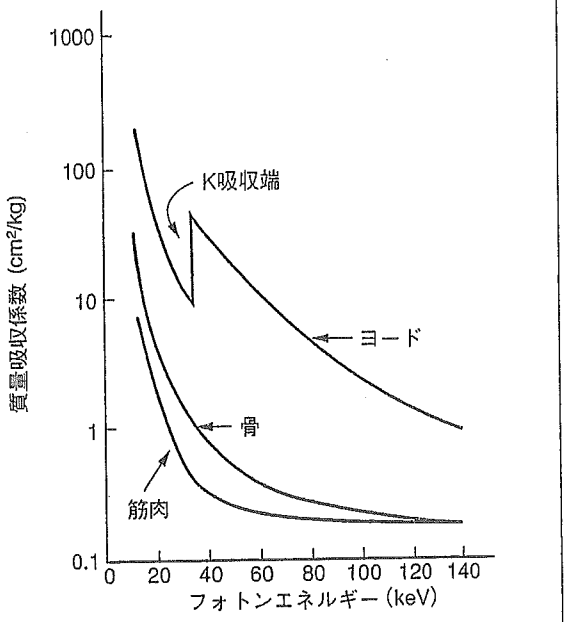

筋肉，骨およびヨードのK吸収端の関係。ヨードのK吸収端は33.3keVで上昇するため，その直上で人体との組織吸収係数の差が最大となる。

図❷　病院設置型微小血管造影装置

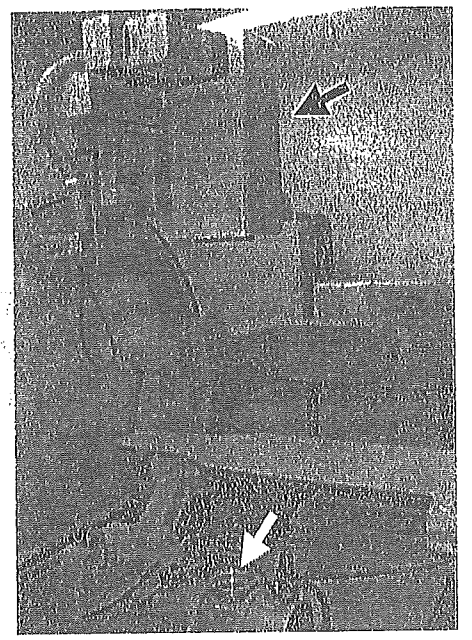

NHKの高感度・高精細撮像管であるアバランシェ型ハイビジョンモノクロ新Super-HARPカメラ（黒矢印）とCT用のX線管を転用した高出力線源（白矢印）から構成されている。

平行に近い性質がある。単色光の利点として，ヨードは33.3keVのエネルギーレベルでK吸収端を持つ。これは質量吸収係数が不連続に上昇し，X線のエネルギーをヨードのK吸収端の直上のエネルギーに変換すると，ヨードと周囲組織との質量吸収係数の差が最大となる（図❶）。組織とヨードとのコントラストが最良となるため，微量のヨードを検出できやすくする効果がある。放射光のX線は，既存のX線装置より約108倍以上も輝度が高く，シリコン結晶を用いてヨード吸収端の直上に設定することにより，単色化しても十分なフォトン量を維持することが可能である。検出系は高解像度・高感度蛍光板で作製した蛍光像を，超高感度・高精細撮像管であるアバランシェ型ハイビジョンモノクロ新Super-HARPカメラで撮影する。これらの検出器系から高解像度微小血管造影像（50 μm）が得られる[5)-8)]。既存の撮影装置のようにイメージインテンシファイヤーとCCDカメラを用いた検出器では，感度と解像度が低いため，高精細画像として微小血管を描出するには限界がある。

2．病院設置型微小血管造影法

放射光施設は多額のコストと広大な敷地を必要とし，臨床導入するには時間的・空間的にも問題がある。そこで微小血管造影法が臨床応用できるように，新エネルギー・産業技術開発機構（NEDO）の支援により，病院設置型の微小血管造影装置を浜松ホトニクス・NHKエンジニアリングの協力を得て共同開発した。X線管は最大陽極熱容量が5MHUと世界最大級の大きさであるCT用管球を転用した（図❷）。X線高電圧装置も大出力化し，市販の装置では不可能な70kVp・800mAで高輝度のX線を連続20秒間まで撮影できる。疑似単色化はランタノイド系の金属を複合したフィルターで，ヨードのK吸収端である33keV付近に頂点を有し，約20keVのバンド状の照射X線スペクトルに変換した。検出系は，放射光微小血管造影法と同じ，NHKの高感度・高精細撮像管であるアバランシェ型ハイビジョンモノクロ新Super-HARPカメラを用いている。

安全性の検討として，照射X線量と散乱X線量

図❸ プラズマX線微小血管造影装置（文献9より改変）

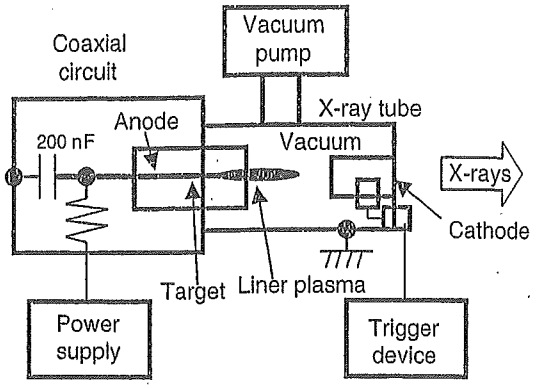

高電圧コンデンサーに約50～60V充電すると，陽極のターゲット金属が気化されプラズマを形成する。トリガ装置によりX線管内へ放電し，擬似単色X線を発生させる。

図❹ プラズマX線の発生原理（文献9より改変）

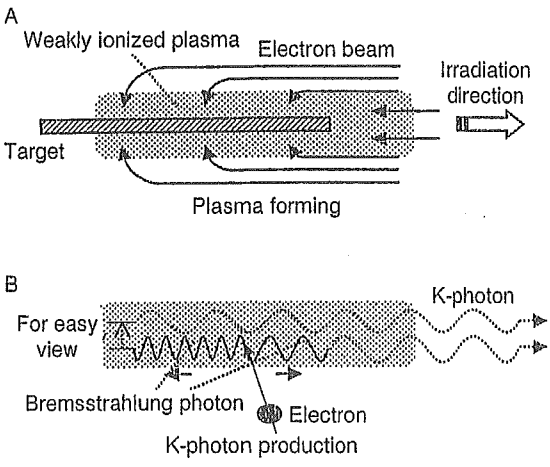

A. 高エネルギー放電により弱電離プラズマX線源を成長させ，線状に形成することにより制動X線を特性X線に変換する。
B. K系列線はL系列線と比較して，制動X線から特性X線への変換率が高い。

を計測した。X線発生装置から1mに検出器を設置し，管電圧70kV，管電流500mAで20秒照射した場合，0.547Sv（62.7R）であった。検査の撮影条件としては最低でも1検査あたり100R以下（3R/sec）を目標としており，妥当な線量と考えられる。また，X線発生装置から1mの距離にファントムを置き，50cm側方で散乱X線を検出した場合の散乱X線量は0.0225mSv（2.58mR）であった。放射線医療従事者の年間被曝量の限度は50mSvであり，許容範囲内と考えられる。本装置は，2004年3月に国立循環器病センターに設置され，医師主導のもと，臨床応用が開始される。

3．プラズマX線微小血管造影法

装置は高電圧電源，高電圧コンデンサー，プラズマX線管からなり，高電圧コンデンサーの容量を増すことによりX線の高輝度化が可能となる（図❸）。プラズマX線はシャープなK系列特性X線であり，その発生原理は高エネルギー放電により弱電離プラズマX線源を成長させ，線状に形成することにより制動X線を特性X線に変換する。特性X線はプラズマを容易に通過するので，高線量の疑似単色X線が発生する（図❹A）。さらに，K系列特性線は蛍光吸収率が高いので，L系列線と比較して制動X線から特性X線への変換率が高い（図❹B）。プラズマX線は金属ターゲットの種類により，特性X線のエネルギーを任意に選択することができる。例えば，セリウムを陽極に用いると約34keVの特性X線を得られ，ヨードのK吸収端である33keV直上のエネルギーを持つ擬似単色X線での撮影が可能となる[9]。

Ⅱ．微小血管の画像による評価

1．正常血管と再生血管の比較

Takeshitaらは，放射光微小血管造影装置を用い，ラットの大腿動脈を結紮した後の再生血管と結紮処置をしていないコントロールの血管性状を比較した[10]。結紮してから4週後に血管撮影をした結果，線状とらせん状の2種類の血管が存在したが，コントロールでは線状の血管のみであり，らせん状の血管は観察されなかった。このことから，再生される血管には線状とらせん状の2種類の構造を持つ血管があるが，線状の血管は既存の血管であった可能性もあると示唆した。しかし，らせん状の血管はコントロールでは観察されないため，少なくとも虚血により再生した結果で生じた血管であるとしている。また，血管内皮依存性の血管拡張薬であるアセチルコリンを投与した場合，線状の血管は拡張するものの，らせん状の血管は拡張しなかった。さらに，血管内皮増殖因子である

図⑤　再生血管のアデノシン投与による反応

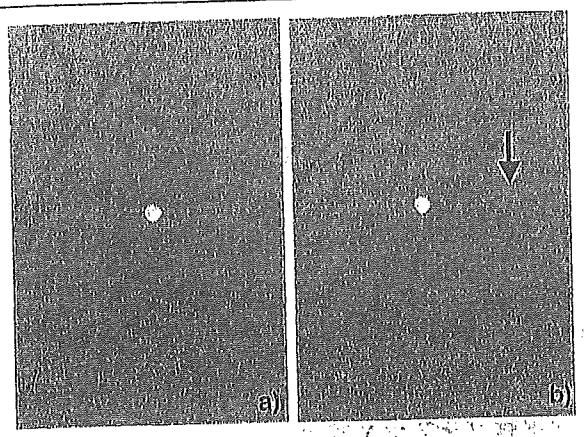

FGF-4-ゼラチンハイドロゲル複合体で治療したウサギ下肢の微小血管造影。アデノシン投与前（a）とアデノシンの投与後（b）。らせん状の血管が拡張するのが観察できる（矢印）。

vascular endothelial growth factor（VEGF）で治療したラットで観察されたらせん状の血管も拡張せず[11]，以上のことから虚血により生じた再生血管やVEGFにより再生したらせん状の再生血管は，内皮機能が備わっていない不完全な再生血管であると考えられた。一方，fibroblast growth factor 4（FGF-4）-ゼラチンハイドロゲル複合体にて血管再生治療後のウサギの下肢虚血モデルを撮影した。観察されている血管は再生血管と考えられ，アデノシンの投与によりらせん状の血管が拡張したと報告されている[12]。病院設置型の微小血管造影装置でも同様に，FGF-4-ゼラチンハイドロゲル複合体で治療した場合，アデノシンの投与によりらせん状の血管が拡張した（図⑥）。これにより，FGF-4-ゼラチンハイドロゲル複合体で治療した場合には，より成熟した血管が再生したと考えられる。

2．病院設置型とプラズマX線微小血管造影装置

病院設置型の微小血管造影装置のX線源では，その単色X線光子数の限界から，現在は体厚が8cmの下肢の微小血管造影に対象が限られている。

図⑥　既存のX線装置とプラズマX線装置の比較

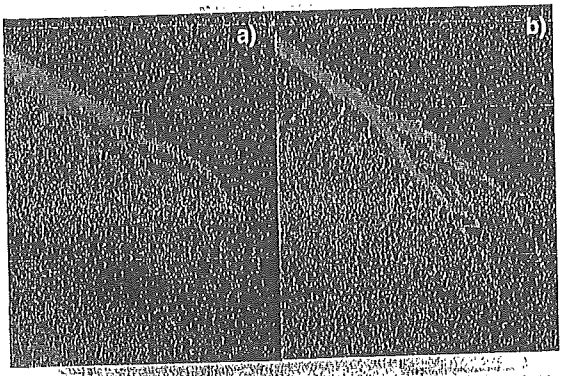

イヌ冠動脈ファントムの血管造影。既存のX線装置では心筋貫通枝は観察できないが（a），プラズマX線装置では詳細に観察が可能である（b）。

体厚が8cm程度の被写体では微小血管を描出できるが，10cmを超えると血管像をほとんど得ることができない。一方，プラズマX線装置は，コンデンサーの容量を増加させることで，高輝度化することが可能であるため，人体を通過する疑似単色X線が得られる可能性があると考えられている。マイクロスフィアーを充填したイヌ冠動脈ファントムをプラズマX線装置と既存の血管造影装置とで比較した場合，プラズマX線で撮影した場合は心筋貫通枝レベルのミクロンオーダーの微小血管が詳細に観察できたが，既存の血管造影装置では観察できなかった（図⑥）。

おわりに

微小血管造影法にて観察されている血管は，必ずしも新生血管とは限らず，側副血行路の血流の増加やあらかじめ存在していた微小血管の拡張であるかもしれないということを忘れてはならない。しかし，微小血管造影法による画像評価は，血管の種類や反応性の評価まで可能となる。今後の臨床導入により，さらに詳細に検討されることを期待している。

用語解説

1．**血管再生治療**：虚血性疾患において，血行再建や薬剤治療に抵抗する症例に対し，新生血管を形成させ，血流を改善させる治療である。現在は，自己骨髄やサイトカインなどを用いて臨床応用されている。

2．**微小血管造影法**：既存の血管造影装置の空間解像度は200～300μmであるが，100μm以下の解像度を持つ撮影装置にて微小血管の造影が可能となっている。血管再生治療で再生された血管の評価に期待されている。

参考文献

1) Asahara T, Murohara T, et al : Science 275, 964-966, 1997.
2) Shintani S, Murohara T, et al : Circulation 103, 897-903, 2001.
3) Tateishi-Yuyama E, Matsubara H, et al : Lancet 360, 427-435, 2002.
4) Mori H, Hyodo K, et al : Circulation 89, 863-871, 1994.
5) Tanioka K : Proc SPIE Int Soc Opt Eng 1656, 1-12, 1992.
6) Kubota M, Kato T, et al : IEEE Trans Broadcasting 42, 251-258, 1996.
7) Umetani K, Ueki H, et al : J Synchrotron Rad 5, 1130-1132, 1998.
8) Tanioka K, Ohkawa Y, et al : IEEE Workshop on CCD and Advanced Image Sensors, 2001.
9) Sato E, Hayasi E, et al : SPIE 4682, 538-548, 2002.
10) Takeshita S, Isshiki T, et al : Circulation 95, 805-808, 1997.
11) Takeshita S, Isshiki T, et al : Circulation 98, 1261-1263, 1998.
12) Kasahara H, Tanaka E, et al : J Am Coll Cardiol 41, 1056-1062, 2003.

参考図書

＊機能・代謝画像診断法と分子画像，西村恒彦 編，南山堂，2003.
＊INNERVISION 17(8)，疑似X線レーザーを用いた普及型微小血管造影装置の開発，知久正明，西上和宏 他，インナービジョン，2003.

参考ホームページ

・大型放射光施設SPring-8
http://www.spring 8.or.jp/j/
・高エネルギー加速器研究機構
http://www.kek.jp/ja/index.html

知久正明
1994年：日本大学医学部卒業後，日本大学第二内科入局
1996年：日本大学医学部大学院入学
2000年：大学院卒業後，国立甲府病院循環器科に勤務
2003年：国立循環器病センター修練医
現在は，大血管疾患から末梢血管疾患の非侵襲的診断法および血管再生治療における微小血管造影法の研究を行っている。

X-BAND LINAC BEAM-LINE FOR MEDICAL COMPTON SCATTERING X-RAY SOURCE

Katsuhiro Dobashi, National Institute of Radiological Sciences, Chiba, Japan
Mitsuru Uesaka, Atsushi Fukasawa, Futato Ebina, Tatsuo Kaneyasu,
Haruyuki Ogino, Fumito Sakamoto, Tomohiko Yamomoto, UTNS University of Tokyo, Ibaraki, Japan
Junji Urakawa, Toshiyasu Higo, Mitsuo Akemoto, Hitoshi Hayano, KEK, Tsukuba, Japan

Abstract

Compton scattering hard X-ray source for 10-40 keV are under construction using the X-band (11.424 GHz) electron linear accelerator and YAG laser at Nuclear Engineering Research laboratory, University of Tokyo. This work is a part of the national project on the development of advanced compact medical accelerators in Japan. National Institute for Radiological Science is the host institute and U. Tokyo and KEK are working for the X-ray source. Main advantage is to produce tunable monochromatic hard (10-40 keV) X-rays with the intensities of 10^8-10^9 photons/s (at several stages) and the table-top size. In addition, dual energy monochromatic X-ray source can be realized that generate two monochromatic hard X-ray by turin with high (up to 10 pps) repetition rate by one X-ray source.

The X-ray yield by the electron beam and Q-switch Nd:YAG laser of 2.5 J/10 ns is 10^7 photons/RF-pulse (10^8 photons/sec in 10 pps). X-band beam line for the demonstration is under commissioning. We also design to adopt a technique of laser circulation to increase the X-ray yield up to 10^8 photons/pulse (10^9 photons/s).

INTRODUCTION

Hard X-rays of 10-40 keV are now very useful in medical science, biology and material science. for exaple, Dynamic IVGAC[1, 2] and monochromaticd X-ray imaging, CT. In addition, Dual energy X-ray CT[3] and Substruction imaging with contrast agent and Dual energy X-ray are realized that require two monochromatic hard X-ray.

Intense hard X-rays are generated by a third generation light source. However, most SR sources are too large to be applied and used widely for public usage of the monochromatic hard X-ray. Therefore, we are developing a compact monochromatic hard X-ray (10-40 keV) source based on laser-electron collisions with the X-band (11.424 GHz) linac system[4]. One to ten percent narrow band X-rays are generated by collimating scattered photons that are related to the energy and scattering angle.

The final target of this study is an integrated system for medicine. as shown in Fig.1. This system is equipped with an X-band RF-source and a moving arm including an X-band linac, Q-switch laser system and X-ray detector.

A multi-bunch electron beam generated by a thermionic-cathode RF gun is collimated and compressed temporally by an alpha-magnet and accelerated by X-band accelerating structures. The electron beam is bent by the achromatic bends and focused at the collision point(CP). About a 10 ns hard X-ray is generated via Compton scattering upon laser-electron collision. After the collision, the electron beam is bent and decelerated by an X-band decelerating structure. The decelerated electron beam with an energy lower than 1 MeV is injected to a beam dump. In addition, this system can generate dual energy monochrmatic hard X-ray using two Nd:YAG laser by turn.

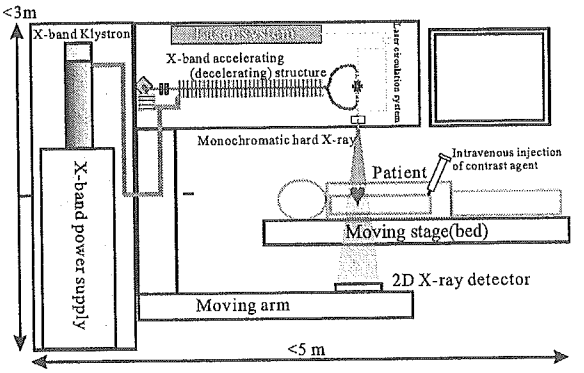

Figure 1: Final target of this study.

The laser system for collision is composed of a Q-switch Nd:YAG laser and a laser pulse circulating system to increase X-ray yield.

To demonstrate that the proposed X-ray source can be realized and will be useful in medicine, an X-band linac beam line for the proof-of-principle experiment shown in Fig. 2 is under construction. The X-ray yield by the electron beam and Q-switch Nd:YAG laser of 2.5 J/10 ns is 10^7 photons/RF-pulse (10^8 photons/sec in 10 pps). X-band beam line for the demonstration is under commissioning. We also design to adopt a technique of laser circulation to increase the X-ray yield up to 10^8 photons/pulse (10^9 photons/s).

In this paper, we present the design and numerical analysis of the X-ray source system to demonstrate hard X-ray generation and its applications.

X-BAND BEAMLINE FOR PROOF-OF-PRINCIPLE EXPERIMENT

Compact hard X-ray source based on the X-band linac that we propose is shown in Fig. 2. Multi-bunch beam generated by thermionic-cathode RF-gun is accelerated by X-band accelerating structures. The beam is bent and focused at the collision point. About 10 ns hard X-ray is generated via Compton scattering on laser-electron collision.

0-7803-8859-3/05/$20.00 ©2005 IEEE

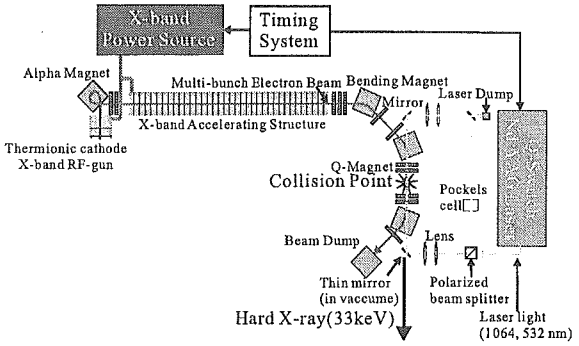

Figure 2: Schematic illustration of Compact Hard X-ray source based on thermionic-cathode X-band RF-gun, X-band accelerating structure and Q-switch Nd:YAG laser.

Beam energy	35 MeV
Charge/bunch	20 pC
bunches/RFpulse	10^4
Beam size(rms)(x,y)	100, 100 μm
Beam emittance(x,y)	10, 10 πmm·mrad

Table 1: Beam parameters at the collision point

X-band linac

X-band linac is applied to the compact hard X-ray source. RF-wavelength of the X-band is 1/4 of S-band (2.856 GHz). However, the maximum filed gradient as $\sim$ 40 MV/m enable remarkable compactness.

An X-band accelerating structure with 0.7 m long is used for the X-ray source. The technologies for X-band accelerating structure developed for future linear colliders[7] at KEK and SLAC are fully adapted for this development. At first, the RDS type accelerating structure has been adopted, which is already under manufacturing.

We adopt PPM type X-band Klystron (E3768A) designed for linear colliders[7]. Klystron Modulator is under design to fit this X-ray source. RF power is above 50MW in 1 μs.

The beam optics of the X-band linac beam line designed using SAD[8] code is shown in Fig.3. Beam parameters at the collision point (CP) are shown in Table 1.

Laser system

To concentrate on R&D of the accelerator, we choose a commercial and reliable laser for laser-electron collision.

To realize such a compact system, we adopt two Q-switch Nd:YAG laser with the intensity 2.5 J/pulse(1.4J/pulse for second harmonics), the repetition rate 10 pps, the pulse length 10 ns(FWHM) and wavelength of 1064 nm(fundamental).

In second step, to switch the X-ray energy immediately, we add the laser system. Each laser system for fundamental and second harmonics are shot by turn. Then we can generate dual energy monochromatic X-ray by turn with repetition rate of 12.5 Hz as shown in Fig.4. Advantage

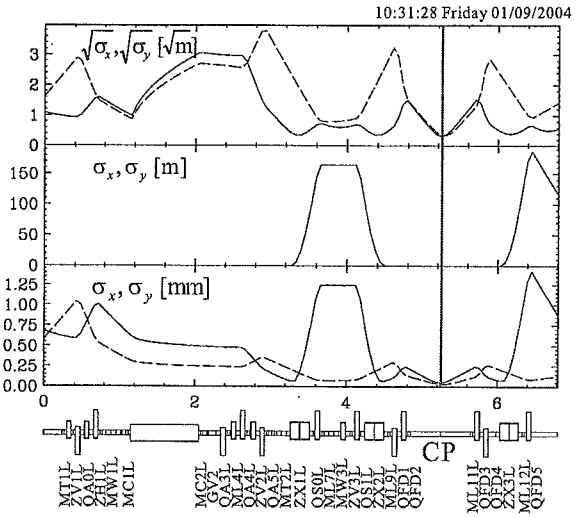

Figure 3: Beam optics for X-band linac.

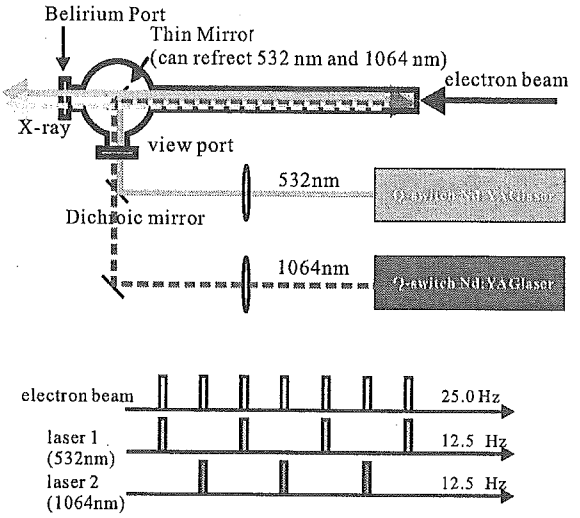

Figure 4: Concept of dual energy X-ray generation system.

of the this dual energy X-ray source is the switing of X-ray energy with high repetition rate that is very useful for dynamic sustructon imaging and dual energy X-ray CT.

To increase X-ray yield, we have to design the technique of circulation of laser pulse, which enhance the luminosity by 10 times. Detail of the laser pulse circulation system will be report in another paper.

X-ray yield and properties

The X-ray yield per bunch is calculated with cross section of Compton scattering and Luminosity. Enegy distributions and energy due to scattering angle of the X-ray for each wavelength of laser light with electron beam energy 35MeV are shown in Fig.5. Property of the X-ray is summalized in Table 2

Figure 6 shows the mean energy and rms energy spread of the available X-ray for each laser wavelength when scat-

0-7803-8859-3/05/$20.00 ©2005 IEEE

laser wavelength (nm)	1064	532
pulse energy of laser (J/pulse)	2.5	1.4
Xray yield (photons/pulse)	9.9×10^6	4.4×10^6
Maximum X-ray energy(keV)	21.9	43.8

Table 2: Properties of the generated X-ray with electron beam energy 35 MeV, charge 20 pC/bunch

tered photon are collimated with each collimated angle.

TEST OF X-BAND RF SOURCE AND X-BAND THERMIONIC CATHODE RF-GUN

Test of RF generation and RF aging of the X-band klystron is under way. Peak power of RF is estimated to 10 MW per RF output port of the klystron. Total output power is 20 MW and pulse length 600 ns, repetition rate 5 pps.

After RF parameters ware reached to required by the RF-gun experiment, we started RF-aging of the X-band thermionic cathode RF-gun. Detail of the exprtiment will be shown in another presentaion.

Next of the RF-gun experiment, Klystron aging is continuled to reach the RF parameter upto 50 MW, 1 μs, 5 pps. Then, X-band acceleratinc structure is installed and acceleration test and X-ray generation will be performed at this autumn.

APPLICATION

Many application of monochromatic hard X-ray is proposed and performed with 3rd generation SR source. Main purpose of this study is demonstration of these applicaton in proposed X-ray source.

After the X-ray generation experiment, we start the experiment for application, for example, Dual energy X-ray CT. Detail of the applicaton experiment is reported in another presentation.

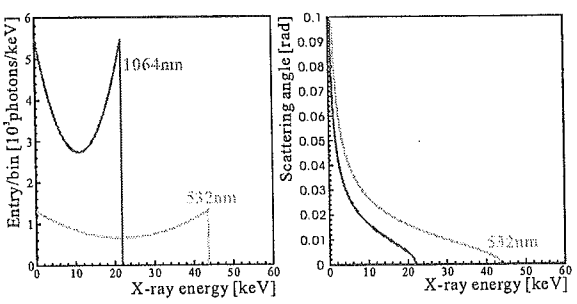

Figure 5: Energy spectrum of X-ray for laser wavelength of 1064 and 532 nm with electron beam energy 35 MeV.

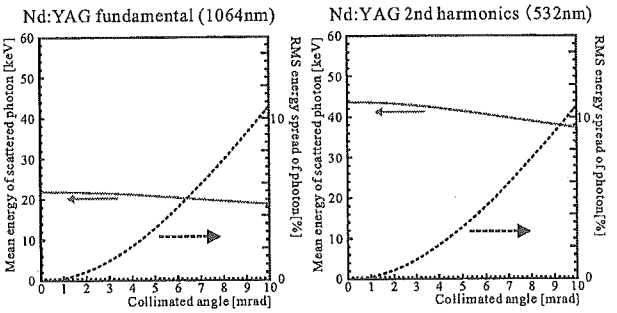

Figure 6: Energy spred in rms and mean energy of available X-ray with each collimated angle.

CONCLUSION

We are developing the compact X-ray source by laser-electron collision based on the X-band linac for medicine. To realize a remarkably compact system, we adopt the X-band system and commercial Q-switch laser. The X-ray yield by the electron beam and Q-switch Nd:YAG laser of 2.5 J/10 ns is 10^7 photons/RF-pulse (10^8 photons/sec in 10 pps). We also design to adopt a technique of laser circulation to increase the X-ray yield up to 10^8 photons/pulse (10^9 photons/s).

Final target of this study is the integrated system for medicine shown in Fig. 5. This system has X-band RF-source and moving arm including X-band linac, Q-switch laser system and X-ray detector. We can perform dynamic IVCAG so as to CAG and can get clear dynamic image of coronary artery with less distress for patients.

ACKNOWLEDGEMENTS

This study is performed in the national project of "Development of Advanced Compact Accelerators" in Japan, partially supported by Research Program on Development of Innovative Technology (#0494) in Japan Science and Technology Agency.

REFERENCES

[1] E. Rubenstein, et al. *Proc. National Academy Sci. USA* **83**(1986)24, p.9724.

[2] S. Ohtsuka, et al. *British Journal of Radiology* **72**(1999) p.24.

[3] M Torikoshi, et al. *Opt.* **6** 371(2000).

[4] K. Dobashi, et al. *Jpn. J. Appi. Phys.* **444A** pp.1999-2005(2005).

[5] K. Dobashi, et al. *Proc. 8th European Particle Accelerator Conference in Paris*, France, 667(2002).

[6] M. Uesaka, et al. *Proc. XXI International LINAC Conference in Korea*, August 19 - 23, Gyeongju, Korea, 626(2002).

[7] GLC report *KEK report* 2003-7(2003).

[8] K.Hirata; An introduction to SAD(Strategic Accelerator Design), Second Advanced ICFA Beam Dynamics Workshop, CERN 88-04 (1988)

DUAL-ENERGY X-RAY CT BY COMPTON SCATTERING HARD X-RAY SOURCE

Tatsuo Kaneyasu, Mitsuru Uesaka*, Nuclear Professional School, University of Tokyo, Japan
Katsuhiro Dobashi, Masami Torikoshi, National Institute of Radiological Sciences, Chiba, Japan

Abstract

We are developing a compact Compton scattering hard X-ray source by the X-band linac and YAG lasers at Nuclear Professional School, University of Tokyo. The compact hard X-ray source can produce tunable monochromatic hard X-rays for 10 - 40 keV. The monochromatic hard X-rays are very useful in large fields of medical and biological sciences. We are planning to carry out dual-energy X-ray CT, which enables us to obtain 3D distribution of effective atomic number $Z_{\rm eff}$ and electron density $\rho_{\rm e}$ in a matter. The hard X-ray source has an advantage in the dual-energy X-ray CT. The X-ray energy can be changed quickly by introducing a fundamental-frequency and a second-harmonic-frequency lasers. It is indispensable to change the X-ray energy quickly for medical imaging, but it is very difficult to achieve the quickness with a large SR light source and others. The information on the atomic number and electron density will be used for radiation treatment planning as well as for identification of materials in a nondestructive test. We examined applicability of the dual-energy X-ray CT for low to medium Z elements ($Z \leq 38$) by considering the X-ray energy profile generated by the Compton scattering hard X-ray source.

INTRODUCTION

Monochromatic hard X-rays are required in large fields of medical and biological applications. Intense hard X-ray is generated by SR light sources, but most of SR light sources are too large for widely applications. Therefore, a compact hard X-ray source is needed for wide use of monochromatic hard X-ray. We have developed a compact Compton scattering hard X-ray source [1, 2] using an X-band linac as presented in Fig. 1. The compact hard X-ray source can produce tunable monochromatic (1 to 10 % energy spread rms) hard X-rays for 10 - 40 keV. We are planning to perform dual-energy X-ray CT using monochromatic hard X-ray, which enables us to obtain cross sectional image of a material based on effective atomic number $Z_{\rm eff}$ and electron density $\rho_{\rm e}$. Experiments for the dual-energy X-ray CT has been carried out utilizing SR light sources to measure electron density in biological materials [3, 4]. The electron density in a biological material was measured in agreement within 1 % of the theoretical one [3]. We will use the dual-energy X-ray CT for atomic number analysis in a material. For instance, the information on atomic number distribution in a tumor will contribute to treatment planning for advanced radiotherapy. Atomic number images in a plant are needed in plant physiology. In a non-destructive test of radioactive waste, we need to identify elements of a material. So far, the dual-energy X-ray CT has been performed for biological materials which consist of light elements of $Z \leq 20$. To apply the dual-energy X-ray CT for wide-range atomic numbers, we have carried out a numerical simulation and examined the applicability of the method by considering the X-ray profile of the compact hard X-ray source. Furthermore, we are planning to apply the compact hard X-ray source for micro vessel angiography and protein structural analysis.

* uesaka@utnl.jp

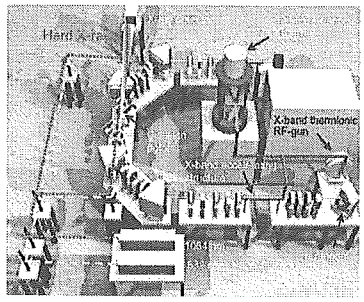

Figure 1: Schematic drawing of the compact hard X-ray source based on Compton scattering.

DUAL-ENERGY X-RAY CT

Theoretical Background

Effective atomic number $Z_{\rm eff}$ and electron density $\rho_{\rm e}$ are obtained by linear attenuation coefficients of a material using two monochromatic X-rays with different energies. A linear attenuation coefficient μ of a material is approximately written as a function of atomic number Z and X-ray energy E using a formula proposed by Jackson and Hawkes [6], as follows;

$$\begin{aligned}\mu(Z,E) \simeq & \rho\frac{N_{\rm A}}{A}Z\{4\sqrt{2}Z^4\alpha^4(\frac{mc^2}{E})\phi_0\sum_{nll'}f_{nll'} \\ & + \sigma_{\rm KN} + \frac{Z(1-Z^{b-1})}{Z'^2}\sigma_{\rm SC}^{\rm coh}(Z',E')\} \\ = & \rho_{\rm e}(Z^4F(Z,E)+G(Z,E))\end{aligned} \quad (1)$$

where, ρ is mass density, $N_{\rm A}$ is Avogadro's number, A is atomic mass, $f_{nll'}$ is the collection terms for photoelectric absorption cross section, $\sigma_{\rm KN}$ is the Klein-Nishina cross section and $\sigma_{\rm SC}^{\rm coh}$ is the coherent scattering cross section of the standard element Z' at energy of $E' = (Z'/Z)^{1/3}E$.

0-7803-8859-3/05/$20.00

In the equation, parameter b is proposed to be 0.5 and the standard element is Oxygen [6]. When linear attenuation coefficients are measured for two energies E_1 and E_2, one can extract effective atomic number $Z_{\rm eff}$ and electron density $\rho_{\rm e}$ by solving following equations;

$$Z^4 = \frac{\mu(E_2)G(Z,E_1) - \mu(E_1)G(Z,E_2)}{\mu(E_1)F(Z,E_2) - \mu(E_2)F(Z,E_1)}, \quad (2)$$

$$\rho_{\rm e} = \frac{\mu(E_1)F(Z,E_2) - \mu(E_2)F(Z,E_1)}{F(Z,E_2)G(Z,E_1) - F(Z,E_1)G(Z,E_2)}. \quad (3)$$

The effective atomic number $Z_{\rm eff}$ is defined for a compound or a mixture as;

$$Z_{\rm eff} = \left(\sum_i q_i Z_i^k\right)^{1/k} \quad (4)$$

where q_i is the fractional electron content of ith element in the compound or the mixture and the parameter $k = 4$.

This dual-energy method is limited by the K-edge energy of a material because the equation (1) can not be applied below K-edge energy. We will operate the compact hard X-ray source as electron beam energy is 35 MeV and the wavelength of the laser is 1064 nm and 532 nm. In this situation, the maximum X-ray energies are 21.9 keV and 43.8 keV. The X-ray energy should allow us to identify elements up to $Z = 38$. Energy spread $\Delta E/E$ of the monochromatic hard X-ray generated by SR is in the order of 10^{-4}, but the energy spread in the compact hard X-ray source is expected to be 1 to 10 % (rms), which is dependent on the collimator angle [2]. The energy spread of the X-ray is negligible with SR light sources, but in the case of the Compton scattering X-ray source the energy spread affects the accuracy of atomic number identification.

To examine the applicability of the dual-energy X-ray CT with the compact hard X-ray source, we have performed a numerical simulation for low to medium Z elements ($Z \leq 38$). We adopt linear attenuation coefficients of materials listed in the photon cross section database [7] in the simulation. The geometry of the dual-energy X-ray CT system in the simulation is shown in Fig. 2. We assumed a point light source and the thickness and width of the sample is 1 mm and 20 mm, respectively. In this case,

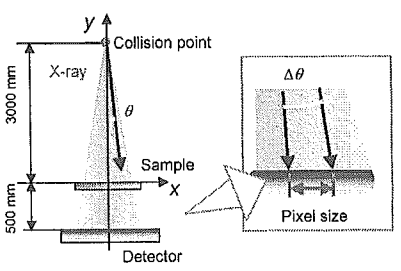

Figure 2: Schematic drawing of the dual-energy X-ray CT system using the compact monochromatic hard X-ray source.

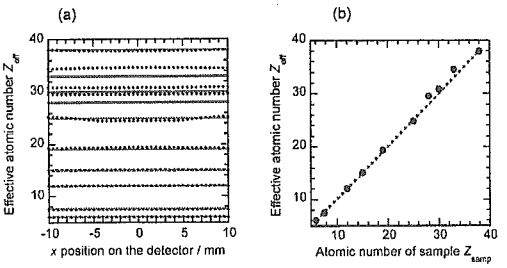

Figure 3: (a) Effective atomic number $Z_{\rm eff}$ on each pixel of the detector. The solid circles indicate identified effective atomic number $Z_{\rm eff}$. (b) Average of the effective atomic numbers.

X-ray photons are collimated at 3.3 mrad. It is noted that the X-ray energy of the Compton scattering X-ray source is dependent on the scattering angle. Thus, the X-ray energy is unique on each pixel of the 2D detector. When pixel size is 0.5 mm, $\Delta\theta$ is less than 0.2 mrad and the energy spread in the pixel is in the order of 0.1 %. This small energy spread in the pixel should improve accuracy of the dual-energy analysis. Effective atomic numbers obtained by the linear attenuation coefficients for two energies on each pixel of the detector are shown in Fig. 3(a). Average of the $Z_{\rm eff}$ is plotted as a function of atomic number of sample $Z_{\rm samp}$ in Fig. 3(b). The accuracy of estimated effective atomic number $\Delta Z/Z$ is less than 3 % (rms) except for $Z = 25$ and 33. We confirmed that atomic number can be identified up to $Z = 38$ using 21.9 keV and 43.8 keV X-rays with enough accuracy even energy spread of the monochromatic X-ray is 1 to 10 %. The limitation of this method is due to K-edge energy of the material.

CT Simulation

A numerical CT simulation has been carried out with low to medium Z elements. We assumed CT system as already shown in Fig. 2 with cylindrical samples. The diameter of the sample is 20 mm and the pixel size of the detector is 0.1 mm. First, light elements of $Z = 13, 15$ and 19 with water as presented in Fig. 4(a) is tested. Reconstructed cross sectional images of the sample based on linear attenuation coefficients are obtained for two energies. Solving the equations (2) and (3), atomic number in the image is derived from linear attenuation coefficients based images. Two-dimensional images based on effective atomic number distribution in the sample and the reconstructed image are shown in Fig. 4. Atomic number distributions of both images at $y = 0$ are compared in Fig. 5(a). As shown in Fig. 5(a), atomic number in the material is well analyzed for light elements of $Z = 13, 15$ and 19 with $\Delta Z/Z_{\rm samp}$ is 2.1, 5.0 and 7.2 % (rms), respectively. The poor accuracy for the element of Z=19 is caused by the reconstruction method and it will be improved.

This analysis can be applied to medium Z elements up to $Z = 38$. We have simulated CT image by assuming a

sample consists of medium Z elements shown in Fig. 6(a). As shown in Fig. 6(b), the medium Z element of $Z = 38$ is also identified with $\Delta Z/Z_{\rm samp}$ is 2.7 % (rms). The atomic number distribution of the reconstructed image at $y = 0$ is compared with that of the sample in Fig. 5(b). We have found that the dual-energy X-ray CT can be used to identify medium Z elements ($Z \leq 38$) in a material using the Compton scattering X-ray source with X-ray energies of 21.9 keV and 43.8 keV.

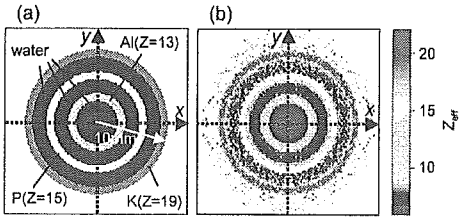

Figure 4: (a) Atomic number distribution in the sample. (b) Atomic number distribution in the reconstructed image.

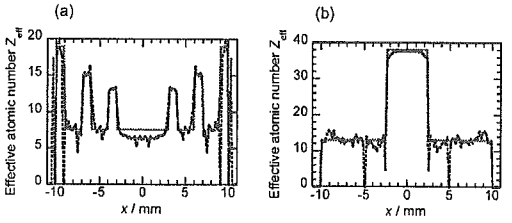

Figure 5: Atomic number distributions at $y = 0$ for sample and reconstructed images in (a) Fig. 4 and (b) Fig. 6. The dotted line indicates effective atomic number $Z_{\rm eff}$ and the solid line indicates atomic number of the sample.

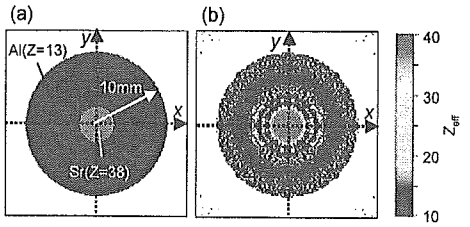

Figure 6: (a) Atomic number distribution in the sample. (b) Atomic number distribution in the reconstructed image.

APPLICATIONS

As already mentioned above, the dual-energy X-ray CT should be a powerful tool for identification of elements in a material. Atomic number distribution measurement will contribute to treatment planning in advanced radiotherapy. We will reveal the availability of atomic number distribution in a tumor using the Monte-Carlo code "EGS4" for a treatment planning. In the biological application, a combination of the dual-energy X-ray CT and the neutron radiography is planned. Neutron radiography enables us to obtain water images in a living plant [5]. The combination of the dual-energy X-ray CT and the neutron radiography is useful to study movement of specific elements in a living plant. The hard X-ray source has an advantage for the dual-energy X-ray CT. The X-ray energy can be changed quickly by introducing a fundamental-frequency and a second-harmonic-frequency lasers. The switching time of the two lasers is planned to be 40 ms. It is needed to change the X-ray energy quickly for the dual-energy X-ray CT in medical and biological applications. Furthermore, the compact hard X-ray source will be applied to micro vessel angiography and protein structural analysis. The micro vessel, diameter of 25 μm, is already observed by SR light. Recently, micro vessel angiography has been performed using X-ray tube combined with the HARP camera in a small laboratory. The micro vessel angiography system will be constructed utilizing the compact X-ray source combined with the HARP camera.

SUMMARY

We have examined the applicability of the dual-energy X-ray CT using the compact hard X-ray source by a numerical simulation. Low to medium Z elements up to Z=38 are well identified with X-ray energies of 21.9 keV and 43.8 keV. Though the energy spread of monochromatic X-ray is 1 to 10 %, the X-ray energy profile depends on the scattering angle. Therefore, the energy spread of X-ray in a pixel is in the order of 0.1 %. The small energy spread in a pixel is an advantage of the Compton scattering X-ray source for the dual-energy X-ray CT. In addition, the X-ray energy can be changed quickly by introducing the two lasers. The quickness is very important advantage of the X-ray source for the dual-energy X-ray CT in medical and biological applications.

ACKNOWLEDGEMENT

The work on development of the X-ray source is performed in the national project of gDevelopment of Advanced Compact Acceleratorsh in Japan and partially supported from Research Program on Development of Innovative Technology in Japan Science and Technology Agency. The study on applications of the X-ray source is supported by the Japanese Ministry of Education, Culture, Sports, Sciences, and Technology and the Japanese Ministry of Health, Labor and Welfare.

REFERENCES

[1] K. Dobashi *et al.*, Proc. 8th European Particle Accelerator Conf. in Paris, France, 2002, p.67.

[2] K. Dobashi *et al.*, Jpn. J. App. Phys. **44** 1999 (2005).

[3] M. Torikoshi *et al.*, Phys. Med. Biol. **48**, 673 (2003).

[4] T. Tsunoo *et al.*, IEEE Trans. NS **50**, 1678 (2003).

[5] T. M. Nakanishi *et al.* J. Radioanal. Nucl. Chem. **255** 149 (2003).

[6] Daphne F. Jackson and D. J. Hawkes, Phys. Rep. **70** 169 (1981).

[7] XCOM http://physics.nist/gov/XCOM

X-BAND THERMIONIC CATHODE RF GUN AT UTNL

A. Fukasawa, T. Kaneyasu, F. Sakamoto, F. Ebina,
H. Ogino, M. Uesaka, UTNL, Naka, Ibaraki 319-1188 Japan
K. Dobashi, NIRS, Chiba, Chiba Japan 263-8555 Japan
J. Urakawa, T. Higo, M. Akemoto, H. Hayano, KEK, Tsukuba, Ibaraki 305-0801 Japan
H. Sakae, K. Matsuo, IHI, Yokahama, Kanagawa 235-8501 Japan

Abstract

A compact Compton scattering hard X-ray source is being developed at Nuclear Engineering Research School (old Nuclear Engineering Research Laboratory). This is considered to be used in the medical scene in the future. This system consists of 50 MeV X-band electron linac and YAG laser to produce 40 keV (fundamental) and 80 keV (the second harmonic). The linac has a thermionic cathode X-band RF gun and an alpha magnet as an injector. Traveling wave tube accelerate the beam up to 50 MeV.

The simulation shows the beam from the gun must be cut off its lower energy part. Alpha magnet with inner slits act as the role, and at the slit position 122 mm energy spread requirement was satisfied, but the charge became small. We must search better operation parameters.

A test beam line to demonstrate production of Compton scattering hard X-ray is under construction. Conditioning of a thermionic cathode X-band RF gun is being proceeded. Feeding with 1.5 MW 100ns was achieved (6 MW 400ns is required for test).

INTRODUCTION

Monochromatic hard X-rays enables advanced diagnostics such as dual X-ray CT[1] and IVCAG[2]. However the spectra of conventional hard X-ray sources are broad since they are bremsstrahlung radiation produced by electrons hitting against targets. A monochrometer can select narrow spectrum but the intensity decreases considerably. Only radiation at storage rings is possible to obtain sufficient intensity through a monochrometer. Its property is very good but the source has difficulty in its huge size for widely use. Compton scattering is one of the solutions to obtain narrow spectrum by putting a hole slit. Since it dose not require a monochrometer, the efficiency to obtain monochromatic X-ray becomes higher.

A compact Compton scattering hard X-ray source for medical use is developing at Nuclear Engineering Research Laboratory (UTNL) [3, 4]. It consists of 50 MeV electron linac and YAG lasers. In the first phase of this study, we will show the validity of our design by the production of Compton scattering hard X-ray. The test beam line is shown in Fig. 1 and the design parameters are in Table 1. The energy spread are required to be less than 1% for focusing at collision point. RF gun is introduced for its low emittance beam production. A thermionic cathode is expected pulse-to-pulse stable operation, although there are problems about backbomberedment. A thermionic carhode RF gun produces multibunch beam (in our case, 10^4 bunches in a 1μs-long RF pulse).

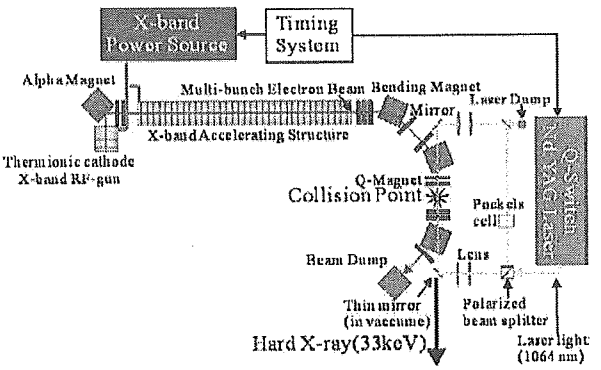

Figure 1: Beam line for a test of Compton scattering.

Table 1: Design parameters

Beam energy	35 MeV
Charge of a bunch	20 pC
Bunches in a pulse	10^4
Normalized emittance	10 πmm.mrad

THERMIONIC CATHODE RF GUN

The injector of this system consists of a thermionic cathode X-band RF gun and an α magnet. An α magnet is used to eliminate low energy particles by its inner slits. Bunch compression is also expected there. Since the energy spread after main acceleration is required to be less than 1%, beams from the injector must satisfy the following equation,

$$\delta = \frac{\Delta E_{inj} + E_{acc}\Delta\phi_{inj}^2}{E} < 0.01$$

where ΔE_{inj} is the energy spread at injector, $\Delta\phi_{inj}$ the bunch length in radians, and E_{acc} the energy gain in the main accelerating structure.

3.5-cell Cavity

Our gun cavity has 3.5 cells (Fig. 3) and is operated at π mode. Coaxial coupler [5] is introduced for axial symmetry of the field in the gun and to place inside solenoid coil. The cathode is dispenser type and the material is tungsten. It will be operated at the current density, 20 A/cm^2.

*fukasawa@utnl.jp

0-7803-8859-3/05/$20.00 ©2005 IEEE

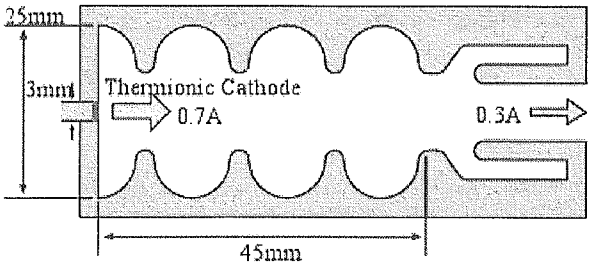

Figure 2: RF gun cavity.

Output of the Gun

The dynamics of the particles in the gun was simulated by PARMELA [6]. The total charge is 41 pC. The bunch length is 4.4 ps and the energy spread 0.16 MeV (those are rms over 2.25 MeV particles) (Fig. 3, 4). Since δ becomes 0.10, lower particles should be eliminated. When the particles less than 2.8 MeV is cut off, the bunch satisfy the energy spread condition (Fig. 5).

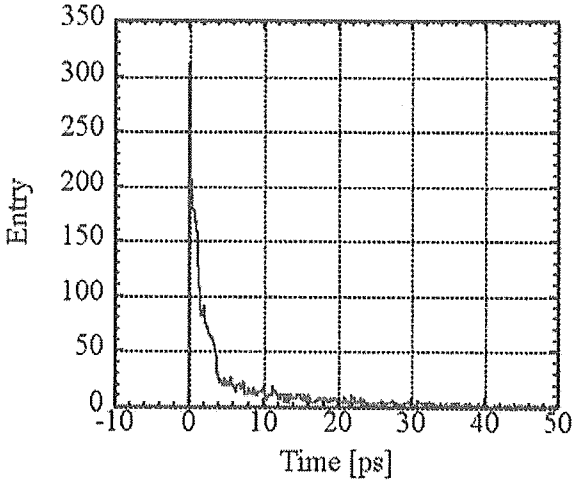

Figure 3: Bunch form (left) before alpha magnet.

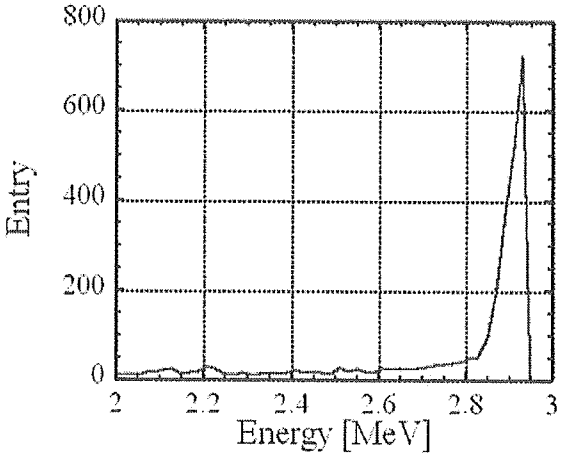

Figure 4: Energy spectrum (right) before alpha magnet.

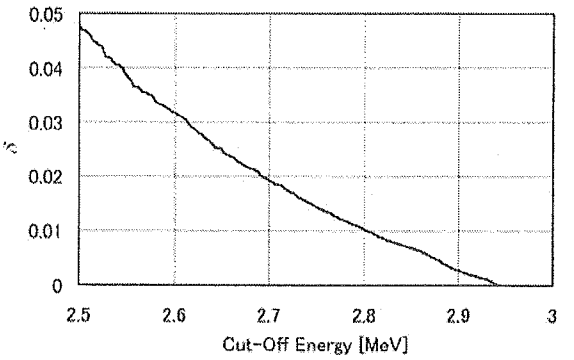

Figure 5: Relation between cut-off energy and estimated energy spread after main acceleration

Slit Position in α Magnet

The motion in the α magnet was calculated next. There is a slit to cut low energy particles in the α magnet. Moving this slit, the cut-off energy can be controlled (Fig.6). The bunch parameters after that are listed in Table 2. When the slit position is 121 mm, the condition is not satisfied. Although 122 mm satisfies it, the charge becomes small. Cut-off energy is higher than estimated in the previous section. This is because over bunching occur in α magnet and bunch length becomes longer. To obtain the best compression and high charge, the field gradient in the α magnet must be higher. However it is difficult to increase the field. Then the energy should be decreased.

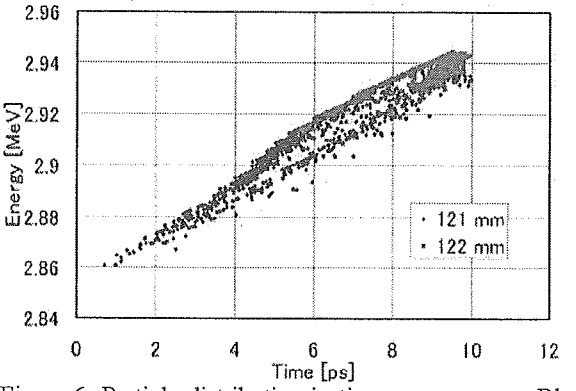

Figure 6: Particle distribution in time-energy space. Blue dots are for the slit position 121 mm and red for 122 mm.

Table 2: Bunch parameters after the α magnet

Position of slit	121 mm	122 mm
Charge	20.2 pC	7.5 pC
Energy	2.92±0.02 MeV	2.94±0.01 MeV
Cut-off energy	2.86 MeV	2.91 MeV
Normalized emittance	15.1, 6.3 πmm.mrad	10.2, 4.1 πmm.mrad
Bunch length	2.2 ps	1.0 ps
δ	0.024	0.005